Int. J. Solids Structures Vol. 29, No. 14/15, pp. 1819–1826, 1992
Printed in Great Britain.

0020–7683/92 $5.00 + .00
Pergamon Press plc

CRACKING IN A LOADED, BRITTLE ELASTIC HALF-SPACE

L. M. KEER and C. H. KUO
Department of Civil Engineering, Northwestern University, Evanston, IL 60208, U.S.A.

Abstract—An approximation giving the relation between the applied load and the crack density in a microscratch test is presented from considerations of sliding contact and fracture analysis. First, the three-dimensional problem of two interacting cracks, with arbitrary shape and configuration, in an elastic half-space is analyzed using the body force method. Then, the analysis is specialized to study the surface cracking which occurs due to the indenter sliding over the rough, brittle half-space. Numerical examples are given for point contact by a spherical indenter sliding over a zirconia ceramic and the shielding effects between two adjacent surface cracks with different spacings are discussed in the context of the determination of crack density.

INTRODUCTION

The microscratch test has become an important technique to characterize the mechanical properties of thin film structures. In the test a nanoindenter is drawn across the surface until some coating failure, adhesive or cohesive failure, occurs at a load which is termed the critical load. Considerable research effort has been directed towards using the scratch test to study the adhesion of thin coatings to substrate (e.g. Valli, 1986; Perry, 1983). The adhesive strength is determined in terms of the critical load at which the coating is stripped from the substrate.

An interesting feature, recently observed by Wu (1990) in a series of microindentation and microscratch tests, is the surface tensile cracks which appear to occur in a regular pattern within the scratch track. Furthermore, a nearly linear relation exists between the applied load and the crack density. By extrapolating the straight line to zero density, the critical load which produces the first crack is obtained. The experimental results reveal that the test may be useful to understanding the cohesive failure properties of brittle materials due to the sliding contact. The objective of this paper is to give a quantitative treatment of the phenomenon of surface cracking in the microscratch test and theoretical interpretation of experimental results when applied to a homogeneous, elastic half-space.

In the present analysis, the three-dimensional crack problem of two interacting cracks in a half-space is first analyzed using the body force method. The configuration and the shape of the cracks may be arbitrary. The crack problem is reduced to a set of coupled singular integral equations with unknown crack opening displacements which are solved numerically by the boundary integral method. Mode I, II and III stress intensity factors for the two cracks are obtained and the results are compared with those presented by Murakami and Nemat-Nasser (1982). The approach is then applied to study the fracture process of surface cracking in a brittle material by considering two interacting parallel surface cracks in a half-space loaded by sliding contact. The approximate crack size and the crack density under various applied loads are estimated.

TWO INTERACTING CRACKS IN A HALF-SPACE

Consider an elastic half-space containing two inclined cracks, D_1 and D_2 as shown in Fig. 1, which are loaded by combined tractions on the crack surfaces. The configuration and geometry of the two cracks may be arbitrary. Two crack coordinate systems, x′ and x″, are introduced here in relation to the global system x. For the three-dimensional crack problem, the body force method has been extensively used to solve the problem of two surface flaws in an elastic half-space (Murakami and Nemat-Nasser, 1982) and a crack

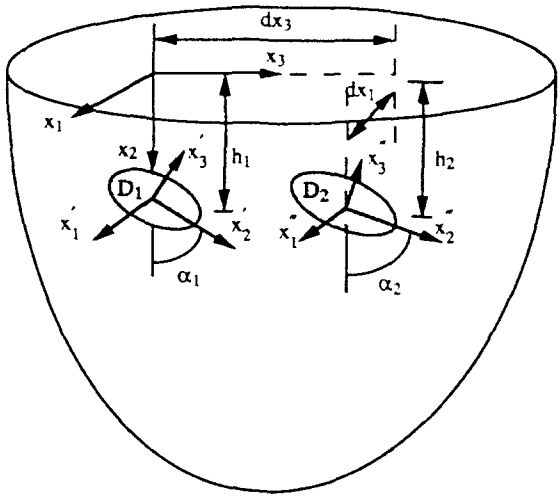

Fig. 1. Two interacting cracks in an elastic half-space.

with arbitrary shape near the interfacial boundary of two-phase material (Lee *et al.*, 1987). The basis of the body force method is to model a crack as a distributed eigenstrain with unknown strength. Appropriate representations of the stress fields in the half-space induced by two cracks, domains Ω_1 and Ω_2 with eigenstrains, ε^{*1}_{mn} and ε^{*2}_{mn}, can be given as

$$\sigma_{ij}(\mathbf{x}) = C_{ijkl}C_{pqmn}\left(\int_{\Omega_1} \varepsilon^{*1}_{mn}\frac{\partial^2 G_{kp}(\mathbf{x},\boldsymbol{\xi})}{\partial x_l\,\partial \xi_q}\,\mathrm{d}\boldsymbol{\xi} + \int_{\Omega_2} \varepsilon^{*2}_{mn}\frac{\partial^2 G_{kp}(\mathbf{x},\boldsymbol{\xi})}{\partial x_l\,\partial \xi_q}\,\mathrm{d}\boldsymbol{\xi}\right). \tag{1}$$

The Green's function $G_{ij}(\mathbf{x}, \boldsymbol{\xi})$ represents the displacement in the x_i direction at point $\mathbf{x}$ caused by a unit body force in the x_j direction at point $\boldsymbol{\xi}$. The boundary conditions for the tractions applied on the crack surfaces can be written as

$$\sigma'_{3i}(x'_1, x'_2, 0) = T'^{1}_i(x'_1, x'_2) \quad (x'_1, x'_2) \in D_1, \tag{2}$$

$$\sigma''_{3i}(x''_1, x''_2, 0) = T''^{2}_i(x''_1, x''_2) \quad (x''_1, x''_2) \in D_2. \tag{3}$$

The superscripts refer to the corresponding cracks and coordinate systems. T'^{1}_i and T''^{2}_i are the applied tractions which can be found from the uncracked solutions. By equilibrating the stress components on the crack surface to the prescribed tractions, a set of coupled singular two-dimensional integral equations are formulated for the unknown crack opening displacements.

$$T'^{1}_i(x'_1, x'_2) = \int_{D_1} b'^{1}_m(\xi'_1, \xi'_2) K^{11}_{im}(x'_1, x'_2, \xi'_1, \xi'_2)\,\mathrm{d}\xi'_1\,\mathrm{d}\xi'_2 + \int_{D_2} b''^{2}_m(\xi''_1, \xi''_2) K^{12}_{im}(x'_1, x'_2, \xi''_1, \xi''_2)\,\mathrm{d}\xi''_1\,\mathrm{d}\xi''_2, \tag{4}$$

$$T''^{2}_i(x''_1, x''_2) = \int_{D_1} b'^{1}_m(\xi'_1, \xi'_2) K^{21}_{im}(x''_1, x''_2, \xi'_1, \xi'_2)\,\mathrm{d}\xi'_1\,\mathrm{d}\xi'_2 + \int_{D_2} b''^{2}_m(\xi''_1, \xi''_2) K^{22}_{im}(x''_1, x''_2, \xi''_1, \xi''_2)\,\mathrm{d}\xi''_1\,\mathrm{d}\xi''_2, \tag{5}$$

where b'^{1}_m and b''^{2}_m are the crack opening displacements for the two cracks. The terms K^{11}_{im} and K^{22}_{im} correspond to the kernel for a single crack, crack 1 and 2 respectively, in the half-space and are given by Lee *et al.* (1987). The kernels K^{12}_{im} and K^{21}_{im} represent the interaction

effect between the two cracks and are derived in the Appendix. A limiting procedure is also applied to shrink the volumes to a planar crack domain: i.e. $\Omega_1 \to D_1$ and $\Omega_2 \to D_2$. The numerical approach to solve the integral equations (4) and (5) is analogous to that developed by Lee *et al.* (1987). The crack front contour is replaced by a straight line segment polygon and the crack surfaces are divided into finite numbers of triangular elements, N_1 and N_2. Since the crack opening displacements vanish in a square root sense as the crack front is approached, accurate results near the crack front are obtained when the crack openings are represented as

$$b_i'^1(\xi_1', \xi_2') = \sqrt{2a^1\varepsilon - \varepsilon^2} f_i'(\xi_1', \xi_2'), \tag{6}$$

$$b_i''^2(\xi_1'', \xi_2'') = \sqrt{2a^2\varepsilon - \varepsilon^2} f_i''(\xi_1'', \xi_2'') \quad i = 1, 2, 3, \tag{7}$$

where ε represents the shortest distance from the integration point to the crack boundary and a^k is a characteristic crack length. The integral equations (4) and (5) are discretized into a set of algebraic equations as

$$\sum_{p=1}^{N_1} K_{impr}^{11} f_{mp}'^1 + \sum_{p=1}^{N_2} K_{impr}^{12} f_{mp}''^2 = T_i'^1(x_1', x_2'), \quad i = 1, 2, 3, \quad r = 1, 2, \ldots, N_1, \tag{8}$$

$$\sum_{p=1}^{N_1} K_{imps}^{21} f_{mp}'^1 + \sum_{p=1}^{N_2} K_{imps}^{22} f_{mp}''^2 = T_i''^2(x_1'', x_2''), \quad i = 1, 2, 3, \quad s = 1, 2, \ldots, N_2. \tag{9}$$

Hence the crack opening displacements and stress intensity factors can be obtained after solving eqns (8) and (9). Numerical results for mode I stress intensity factors of two coplanar surface cracks in the half-space are compared with those obtained by Murakami and Nemat-Nasser (1982). The maximum discrepancy in the results is less than 3%.

SURFACE CRACKING BY SLIDING CONTACT

The scratch test has been commonly used to determine the adhesion of thin hard coatings to substrates. With this method a stylus is drawn across the sample surface under a stepwise or continuously increasing load until a coating failure is found at a certain load, the critical load, and the adhesive strength can be determined in terms of the critical load. The scratch test may cause the coating to fail in several ways, such as spalling, buckling, chipping and cracking and the interpretation of the results from the test is difficult (Burnett and Rickerby, 1987).

A series of microscratch tests has been conducted by Wu (1990) recently to characterize the mechanical properties of thin films. Conical-type diamond nanoindenters with nominal tip radii of 1, 5 and 10 μm were used in the test of ultrathin film structures: a double layer of a 250 Å thick ZrO_2 film on a 250 Å magnetic coating (MC) was deposited on a nickel phosphorous (NiP) substrate. To eliminate the spallation and biaxial stress relief pattern prevailing on the coating surface, the residual stress in the ZrO_2 coating was reduced and the interfacial adhesion between the MC/NiP interface was strengthened by adding a thin Cr (500 Å) adhesive layer. An interesting experimental observation was that surface cracking appeared in a very regular pattern and a nearly linear relation between the crack density and applied load was found. Such a regular crack pattern and spacing as produced by the well-controlled applied loads appears to suggest that the microscratch test may provide an effective approach to determine the mechanical properties of brittle materials and coatings.

In order to estimate these experiments quantitatively, a mechanical model is proposed, as shown in Fig. 2, which represents surface cracking in a brittle material loaded by sliding contact. Although this model is for a monolithic material, later application will be towards coated materials. If it is assumed that the load and friction coefficient are sufficiently large along the surface, then sliding will cause a surface crack to be formed. As sliding commences, a second crack will form, when the shielding effect of the first crack is sufficiently reduced. Thus, for the purposes of the present analysis a two crack system is considered. As shown

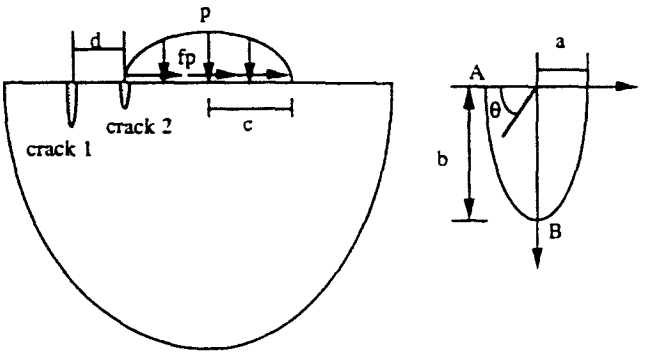

Fig. 2. Surface cracking in the half-space loaded by sliding contact.

in Fig. 2, crack 1 refers to the first or developed crack and crack 2 refers to the shielded crack. Both cracks are assumed to have a semi-elliptical shape with major and minor axes denoted by a and b respectively.

The half-space is assumed to be made of partially stabilized zirconia (ZrO_2) with Young's modulus $E = 200$ GPa, Poisson's ratio $\nu = 0.25$ and fracture toughness $K_{Ic} = 4.82$ $MPm^{1/2}$ (Wilson and Kunz, 1988). A rigid spherical indenter of radius $R = 5$ μm is loaded in sliding contact with friction coefficient $f = 0.5$ on the contact surface. The stress intensity factors of the cracks can be determined by prescribing tractions arising from the contact stresses on the crack faces into eqns (2) and (3). The tractions due to sliding contact are obtained from the undamaged half space solutions, given by Hamilton and Goodman (1966). It is assumed that interaction between the crack and indenter is nil.

RESULTS AND DISCUSSION

When a rough, rigid sphere slides over the surface of a brittle material, the tensile stresses at the trailing edge of the contact may lead to the formation of surface cracks. The cracks may be initiated from small flaws near the surface and further propagation, driven by the subsurface stress field, will cause a change in stress intensity factors along the crack edge and consequently a change of its shape. If the stress intensity factors around the crack front increase with increasing crack size, the growth of the crack will be unstable and the crack will continue to grow until it reaches a state of stable crack growth. Figure 3 gives

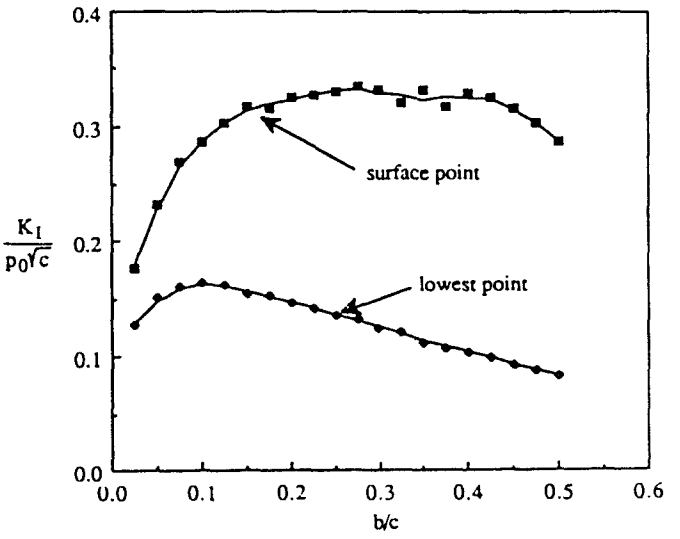

Fig. 3. Mode I stress intensity factors of a semi-circular crack as a function of crack size.

the stress intensity factors, K_I, at the near surface and lowest points of a propagating semi-circular crack, $a = b$, just below the contact edge. The stress intensity factors are normalized to the maximum contact stress and square root of contact radius and the crack size is scaled with the contact radius. It is noted that the stress intensity factors at both points increase with increasing radius, i.e. unstable growth, until the maximum K_I at the lowest point is attained, at radius $b = 0.1c$. The crack is assumed to stop growing downwards at a depth of $b = 0.1c$, while the surface portion continues to grow, since its $K_I > K_{Ic}$. For the case of a thin hard coating deposited on soft substrate, the fracture toughness is generally much higher than that of substrate material and the crack may be arrested at the interface or cause interfacial cracking instead of penetrating through it, unless excessive loading is applied. Thus, the depth of the crack in the hard coating is always less than or equal to the thickness of the coating. It is assumed that the crack will continue to grow, following a semi-elliptical shape, with fixed depth, to reach its stable shape which gives a nearly uniform distribution of stress intensity factor around the crack front. The stress intensity factors at the surface and lowest points of a semi-elliptical crack with the depth of the crack $b = 0.1c$ are shown in Fig. 4. It is found that the values of stress intensity factors at these two points are equal at about $a/c = 0.3$ for which value an approximately uniform distribution of the stress intensity factor around the crack front is attained. Thus the geometry and the size of the initial crack are estimated as a semi-elliptical crack with $a = 0.3c$ and $b = 0.3c$.

Although a series of the cracks is generated in a continuous manner as the indenter slides over the surface, the sliding contact will be modeled approximately to give an estimation of crack spacing. Since the crack spacing represents the distance for a new crack to develop away from the shielding effect of the first crack, the distance between the two cracks is estimated to be the value of tensile stress that can provide sufficient driving force to nucleate a small flaw, i.e. maximum of $K_I > K_{Ic}$. An approximate relation between the crack density and applied load is shown in Fig. 5 by assuming that the shielded crack will initiate from a semi-circular flaw with radius of 0.05 μm. This flaw size is used to demonstrate the method, and different results will be obtained for different assumed flaw sizes, which can be one of the parameters to be sought. It is seen that the relation between load and crack density is not exactly linear as observed by Wu (1990); instead, an abrupt increase in crack density is found for applied loads just beyond the critical load. Thus, the shielding effect that the developed crack imposes on the small flaw appears to be a very local effect, considering the dimensions involved for the crack spacing. Figure 6 shows maximum K_I of the shielded crack as a function of the crack spacing for different applied loads. The

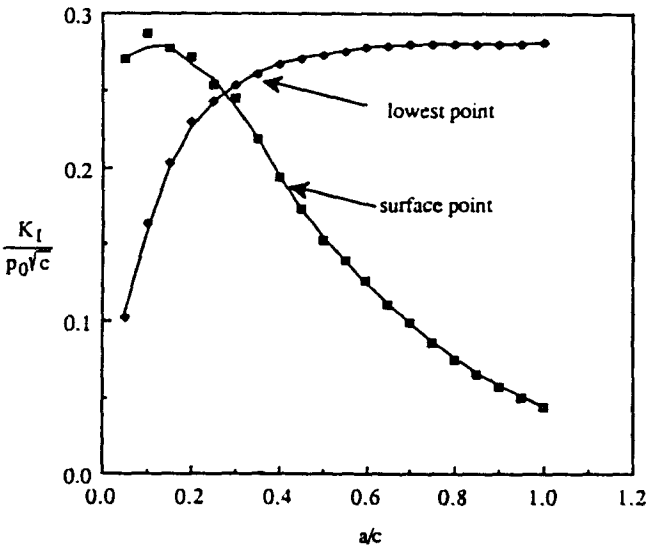

Fig. 4. Mode I stress intensity factors of a semi-elliptical crack as a function of crack size for $b = 0.1c$.

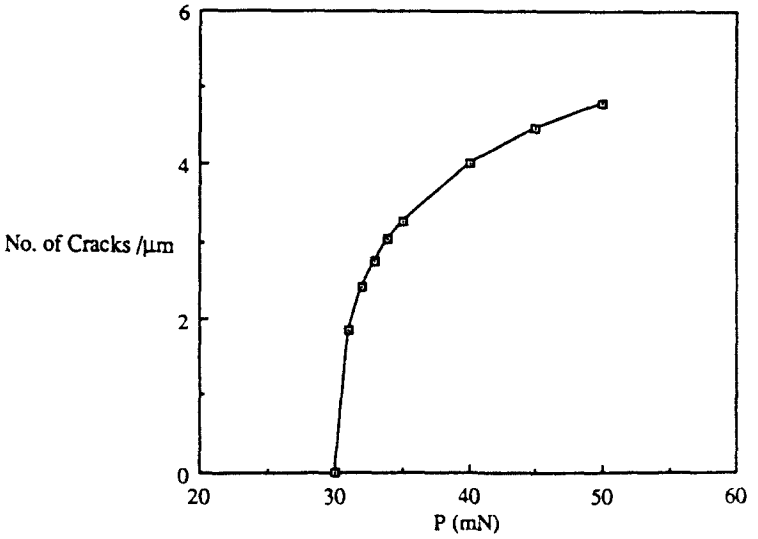

Fig. 5. Crack density as a function of applied load.

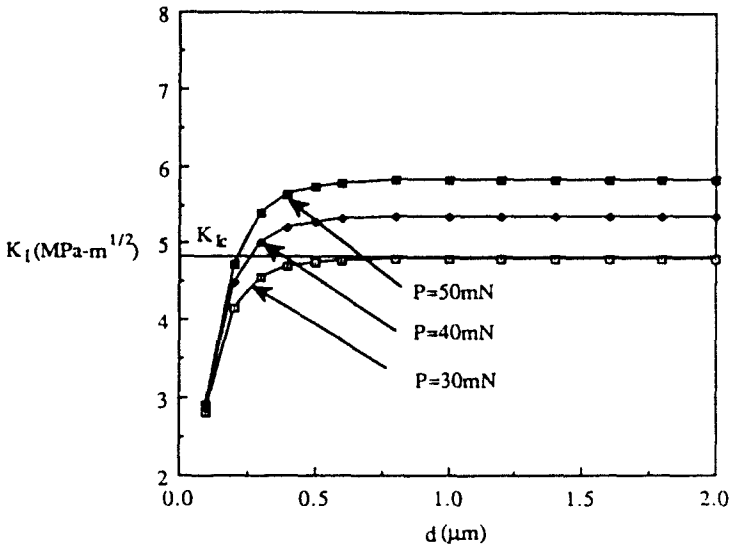

Fig. 6. Maximum K_I of the shielded crack as a function of the crack spacing for different applied loads.

maximum stress intensity factors are less than the fracture toughness (horizontal line) for an applied load less than $P = 30$ mN, the critical load, which corresponds to zero crack density. For the applied loads, $P = 40$ mN and $P = 50$ mN, the distance which corresponds to the intersection of the curve and the fracture toughness is the estimated value of crack spacing, based upon considerations of the two crack interaction. It is also noted that when the crack spacing $d > 0.5$ μm, the shielding effect becomes very small and the problem is returned to the case for a single crack. The stress intensity factors around the crack front of the developed crack are shown in Fig. 7 for different applied loads. The distribution is almost uniform except for the part of the crack near the surface. Figure 8 gives the stress intensity factors around the crack front of the shielded crack under different applied loads. The distributions of the stress intensity factors are almost the same for different loads. The results imply that the shielding effect is a very local phenomenon. From the analysis it is shown that the crack spacing depends on the developed crack size, the critical flaw size of the material to nucleate the crack, and the friction coefficient.

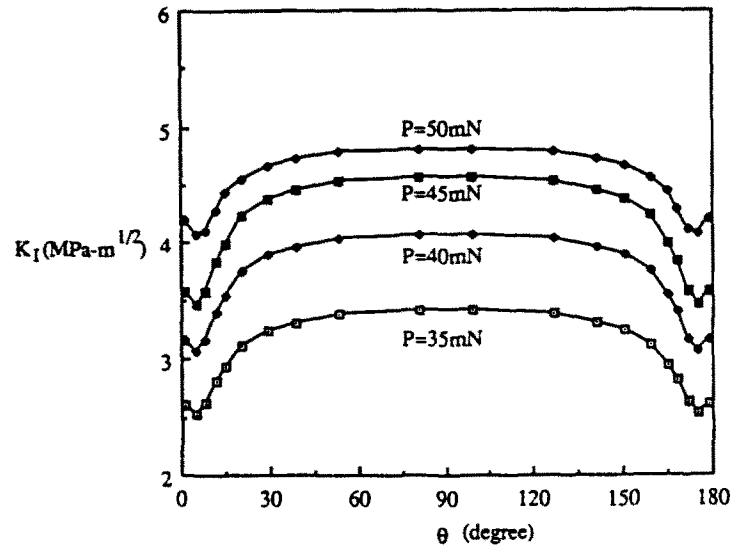

Fig. 7. Mode I stress intensity factors around the crack front on the developed crack under different applied loads.

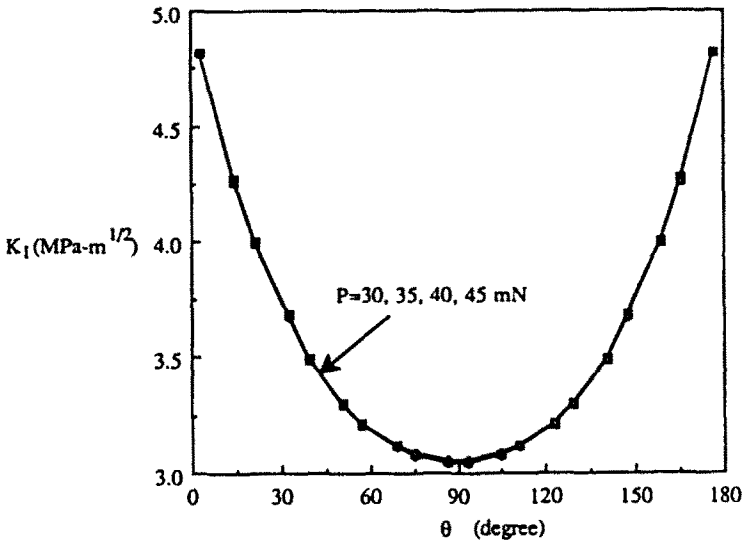

Fig. 8. Mode I stress intensity factors around the crack front of the shielded crack under different applied loads.

CONCLUSIONS

A quantitative analysis of the surface cracking arising from a microscratch test is presented in this paper from considerations of three-dimensional fracture mechanics and sliding contact. The fracture process of such tensile cracks, which occur in a rough tangentially loaded brittle half-space, is studied through a proposed mechanical model which includes the following parameters: crack spacing, crack size, critical flaw size, fracture toughness, friction coefficient and applied stress. The crack spacing is determined from three-dimensional fracture analysis using a predetermined initial crack size, with a given toughness and loaded by rough sliding contact. An approximate relation between the crack density and applied load is obtained by taking account of the shielding between two neighboring cracks. Since the crack spacing is dependent on the developed crack sizes, the critical flaw size of material to nucleate the crack and the friction coefficient, the relation

between crack density and the applied load is not as linear as that found in the experiments performed on thin films. The present model may be useful to study the fracture properties of brittle materials or cohesive strength in the coating and to interpret the experimental observations.

REFERENCES

Burnett, P. J. and Rickerby, D. S. (1966). The relationship between hardness and scratch adhesion. *Thin Solid Films* **154**, 403–416.

Hamilton, G. M. and Goodman, L. E. (1966). The stress field created by a circular sliding contact. *J. Appl. Mech.* **33**, 371–376.

Lee, J. C., Farris, T. N. and Keer, L. M. (1987). Stress intensity factors for cracks of arbitrary shape near an interfacial boundary. *Engng Fract. Mech.* **27**, 27–41.

Murakami, Y. and Nemat-Nasser, S. (1982). Interacting dissimilar semi-elliptical surface flaws under tension and bending. *Engng Fract. Mech.* **16**, 373–386.

Perry, A. J. (1983). Scratch adhesion testing of hard coatings. *Thin Solid Films* **107**, 167–180.

Valli, J. (1986). A review of adhesion test methods for thin hard coatings. *J. Vac. Sci. Technol.* **A4**(6), 3007–3014.

Wilson, J. and Kunz, S. M. (1988). Microwave sintering of partially stabilized zirconia. *J. Am. Ceram. Soc.* **71**, C40–C41.

Wu, T. W. (1990). Microscratch test for ultra-thin films. *Materials Research Society, Thin Films: Stresses and Mechanical Properties II*, **188**, pp. 191–205. Symposium held April 16–19, 1990, San Francisco.

APPENDIX

The set of kernels K_{im}^{12} and K_{im}^{21} are given by the relations

$$K_{ij}^{12}(x_1', x_2', \xi_1'', \xi_2'') = H_{ij}^{12}(x_1', c_1x_2' + h_1, s_1x_2', \xi_1'', c_2\xi_2'' + h_2, s_2\xi_2'' + d_1) \tag{A1}$$

$$K_{ij}^{21}(x_1'', x_2'', \xi_1', \xi_2') = H_{ij}^{21}(x_1'', c_2x_2'' + h_2, s_2x_2'', \xi_1' - d_1, c_1\xi_2' + h_1, s_1\xi_2' - d_1), \tag{A2}$$

where $c_i = \cos\alpha_i$, $s_i = \sin\alpha_i$ and h_i, d_1, d_1 are shown in Fig. 1. The functions H_{ij}^{12} and H_{ij}^{21} can be expressed in terms of second- and fourth-order tensor functions through

$$H_{ij}^{12}(x_1, x_2, x_3, \xi_1, \xi_2, \xi_3) = c_{ip}'c_{jq}'B_{pqmn}(c_{im}''c_{3n}'' + c_{3m}''c_{jn}'') \quad j = 1, 2 \tag{A3}$$

$$H_{i3}^{12}(x_1, x_2, x_3, \xi_1, \xi_2, \xi_3) = c_{ip}'c_{3q}'(A_{pq} + 2B_{pqmn}c_{3m}''c_{3n}''), \tag{A4}$$

where c_{ij}' and c_{ij}'' are the rotations between the crack coordinate systems and the global system and are defined by

$$c_{ij}' = \begin{bmatrix} 1 & 0 & 0 \\ 0 & c_1 & s_1 \\ 0 & -s_1 & c_1 \end{bmatrix} \quad c_{ij}'' = \begin{bmatrix} 1 & 0 & 0 \\ 0 & c_2 & s_2 \\ 0 & -s_2 & c_2 \end{bmatrix}. \tag{A5}$$

The tensor functions are

$$A_{ij} = \lambda^2\delta_{ij}\frac{\partial^2 G_{kp}(\mathbf{x}, \boldsymbol{\xi})}{\partial x_k \partial \xi_p} + \lambda\mu\left(\frac{\partial^2 G_{ip}(\mathbf{x}, \boldsymbol{\xi})}{\partial x_j \partial \xi_p} + \frac{\partial^2 G_{jp}(\mathbf{x}, \boldsymbol{\xi})}{\partial x_i \partial \xi_p}\right) \tag{A6}$$

and

$$B_{pqmn} = \lambda\mu\delta_{pq}\frac{\partial^2 G_{km}(\mathbf{x}, \boldsymbol{\xi})}{\partial x_k \partial \xi_n} + \mu^2\left(\frac{\partial^2 G_{pm}(\mathbf{x}, \boldsymbol{\xi})}{\partial x_q \partial \xi_n} + \frac{\partial^2 G_{qm}(\mathbf{x}, \boldsymbol{\xi})}{\partial x_p \partial \xi_n}\right). \tag{A7}$$

Here, λ and μ are Lamé's constants and δ_{ij} is the Kronecker delta. The functions H_{ij}^{21} can be obtained simply by interchanging c_{ij}' and c_{ij}'' in eqns (A3) and (A4).